ACS OMEGA

Open Access

http://pubs.acs.org/journal/acsodf

Article

Melamine-Derived Mesoporous Carbon for Efficient and Selective Removal of Trace Hg(II) from Honeysuckle Decoction

Qing He, Kun Pang, Lin Tian, Yiqian Ma, Xiang Guo, Jianyong Zhang,* and Ming Yu*

Cite This: *ACS Omega* 2024, 9, 44931−44941

Read Online

ACCESS | Metrics & More | Article Recommendations | Supporting Information

ABSTRACT: Melamine-derived mesoporous carbon, which was obtained from pyrolysis of modified melamine, was employed for the purpose of eliminating trace amounts of Hg(II) from honeysuckle decoction. The specific surface area of the mesoporous carbons with N-functional (MCN_1) was 648.372 $m^2 \cdot g^{-1}$. The chemical composition and morphology of MCN_1 were thoroughly examined, and a comprehensive analysis led to the identification of its formation mechanism. A noteworthy association has been identified between the adsorption efficacy and the chemical composition of MCN_1. In the elimination of trace mercury in aqueous solutions over a broad pH range (pH 2−9), MCN_1 demonstrates high effectiveness, approaching 100%. Adsorption kinetics and isotherm results indicate that a more accurate representation of Hg(II) adsorption on MCN_1 is provided by pseudo-second-order kinetics and Freundlich models, with chemical adsorption being the dominant mechanism. This study further examined the removal of chlorogenic acid, a bioactive component, by MCN_1. The findings imply that MCN_1 has a noteworthy 80% efficacy in removing mercury from honeysuckle decoction while maintaining the purity of its medicinal ingredients, particularly chlorogenic acid. As a result, utilizing MCN_1 for the adsorption of Hg(II) in honeysuckle decoction appears to be a reasonable approach.

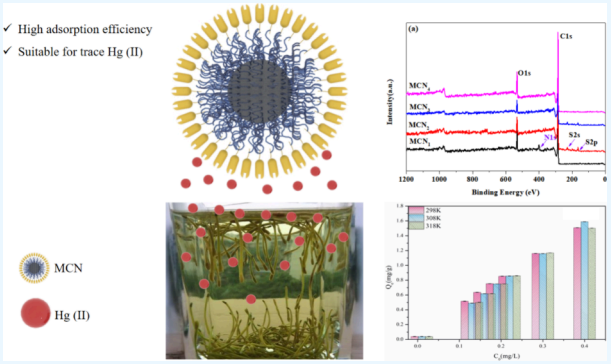

1. INTRODUCTION

Heavy metals have garnered widespread attention globally due to their recalcitrance to biodegradation, propensity for accumulation, migratory nature, and extended half-lives even at trace concentrations, thereby posing a significant threat to human health.[1−3] Hg(II) is considered as a highly toxic heavy metal.[4] When blood mercury(II) levels rise above 200 $\mu g \cdot L^{-1}$, the human central nervous system is directly harmed, leading to paralysis, language difficulties, hearing loss, and even dementia.[5] Multiple studies have indicated a prevalent issue of heavy metal residues in traditional Chinese herbs-(CHMs).[6−11] Contamination of Chinese herbal medicines with heavy metals poses significant health risks to humans and hinders their use and development, as these metals can accumulate in organisms through the food chain.[12,13] Consequently, the heavy metal content within CHMs stands as a pivotal factor influencing their quality and safety.[14]

Lonicera japonica Thunb, which produces honeysuckle flowers and buds, is widely utilized in Traditional Chinese Medicine(TCM) and food products.[15−17] Honeysuckle contains chlorogenic acid, flavonoids, and polysaccharides as its natural active compounds, exhibiting antioxidant, anti-inflammatory, antiobesity, and antitumor properties. However, Bu et al. showed that there were still excessive levels of heavy metals in *Lonicerae japonicae flos* (LJF) medicinal materials and pieces, posing a danger to human health.[18] For a long time, honeysuckle has been potentially harmful to human health due to the accumulation of heavy metals, which has placed certain restrictions on its promotion and application.[19] Therefore, efficient technologies for removing heavy metals. Effective removal of the heavy metal components from honeysuckles is required before their application in clinical settings. This will not only help improve the overall quality of traditional Chinese medicine but will also ensure the safety of medications.[20]

At present, in CHM environments that mimic heavy metal contamination, the primary means of heavy metal removal include coagulation precipitation,[21,22] adsorption techniques,[23,24] molecular sieve filtration, microbial treatment,[25] etc. Adsorption technology, valued for its simplicity, cost-effectiveness, and high efficiency, is a leading method for removing heavy metals from contaminated water and environments.[26−29] There are many kinds of adsorbents used to remove heavy metals from CHMs, mainly including engineered fusion proteins,[25] chitosan,[22] activated carbons,[30,31]

Received: April 5, 2024
Revised: October 21, 2024
Accepted: October 23, 2024
Published: November 1, 2024

and chelating resins,[32] as well as biomimetic materials,[33] mesoporous carbons,[34] etc. In the decoction of Chinese herbal medicines (CHMs), heavy metal content is typically found to be at low levels, while the matrix exhibits a high degree of complexity." This version specifies "Chinese herbal medicines" for clarity and changes "contents".[35] The key to removing heavy metals from CHMs is to ensure that the amount of active ingredients is maintained while doing so, by preserving the effectiveness of the CHMs. Despite the fact that those methods primarily focused on the changes in the constituent parts of CHMs during the removal of heavy metals, there were relatively few studies conducted on the in situ removal of trace metals.

Mesoporous carbon is highly regarded for heavy metal removal due to its high surface area, abundant pores, adjustable active sites, and excellent mechanical and thermal stability, making it an ideal material for water treatment.[36,37] In our previous work,[34] we found that amino-functionalization mesoporous carbon adsorbs approximately 66% of mercury from honeysuckle decoction without altering any of its active ingredients (chlorogenic acid) under optimal adsorption conditions. However, in practical applications, in order to further enhance the absorption rate of mesoporous carbon, it is necessary to refine the porous structure for enhancing its adsorption efficacy. At the same time, in order to guide its practical application, it is necessary to further clarify the specific adsorption mechanism. In this research, we have proposed an N-functional mesoporous carbon obtained from pyrolysis of modified melamine to improve the removal efficiency of Hg (II) in CHMs decoction. Furthermore, a thorough investigation was conducted into the adsorption characteristics and mechanism of N-functional mesoporous carbons as adsorbents for the removal of Hg (II) from aqueous solutions and honeysuckle decoction. A detailed study examined how N-functional mesoporous carbons adsorb Hg(II) from water and honeysuckle decoction, presenting a new, effective mercury(II) removal method.

2. RESULTS AND DISCUSSION

2.1. Characterization of Prepared Mesoporous Carbons. The morphologies of different samples (MCN_1, MCN_2, MCN_3, and MCN_4) are characterized by SEM and TEM images. As shown in Figure 1a,a_1, MCN_1 by using F127 as a soft template shows small uniform spherical particles with a smooth surface, and HR-TEM images show a large number of micropores and mesopores; the particle size is near 1−5 μm. A gradient pore size provides active sites for ion adsorption but also buffers ion movement in rapid motion.[38] As shown in Figure 1b, MCN_2 exhibits a surface with uniform and loose pores, created by using spheres of nano magnesium oxide (nano-MgO) as templates and ammonium citrate as an auxiliary agent at 800 °C activation temperature. At the pyrolysis temperature of 900 °C, part of the pores on the surface of MCN_3 collapsed, indicating that the outer carbon pores collapsed as the pyrolysis temperature increased. When MCN_2 is refluxed in ethanol hydrochloride and oxidized by nitric acid, the carbon layer disappears, and a series of macropores appear in MCN_4, with the pore size becoming larger. To summarize, MCN_1, MCN_2, MCN_3, and MCN_4 exhibit a micro- and mesoporous structure both on the surface and inside.

For further investigation of the pore structure of carbon samples, the N_2 adsorption−desorption isotherms and pore

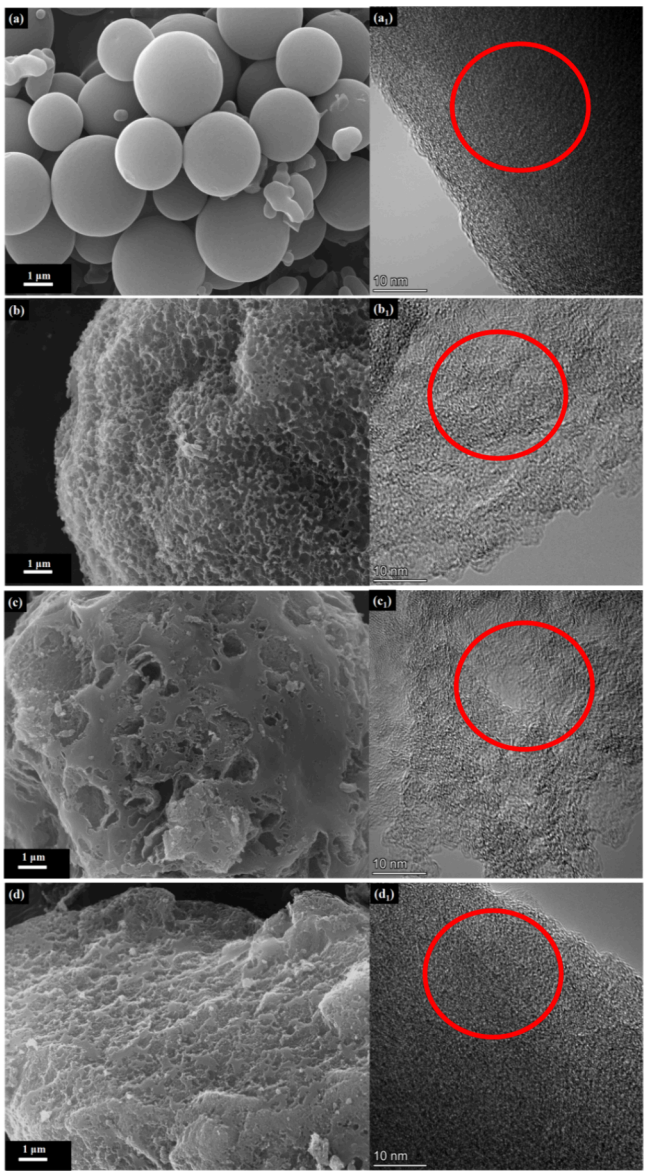

Figure 1. SEM and HR-TEM images of mesoporous carbon (a, a_1) MCN_1, (b, b_1) MCN_2, (c, c_1) MCN_3, and (d, d_1) MCN_4.

size distribution curves for MCN_1, MCN_2, MCN_3, and MCN_4 are shown in Figure 2. In Figure 2, all samples' isotherms are a typical IV(a)-type isotherm, and the occurrence of a hysteresis loop is evident at $0.25 < P/P_0 < 0.85$, suggesting that the samples have a mesoporous structure.[39] The materials still adsorb at $P/P_0 < 0.2$, affirming the presence of micropores.[39] In Table 1, parameters describing the pore structure are listed. N_2 adsorption/desorption isotherm measurements illustrate that these MCN_1 exhibited relatively high specific surface areas of 648.372 $m^2 \cdot g^{-1}$ and an average pore size of about 3.366 nm, as calculated by the Barrett−Joyner−Halenda (BJH) method. The specific surface areas of MCN_2, MCN_3, and MCN_4 are 1197.054, 1403.363, and 1517.485 $m^2 \cdot g^{-1}$, respectively. Also, the average pore size of samples ranges from 2.558 to 5.017 nm. The findings indicate that for MCN_1 the majority of the samples primarily consist of mesopores with a small number of micropores, aligning with the outcomes from TEM and SEM examination. The approximate D_{BJH} of MCN_1 and MCN_4 is near 3.3 nm, demonstrating that it could provide the same

https://doi.org/10.1021/acsomega.4c03269
ACS Omega 2024, 9, 44931−44941

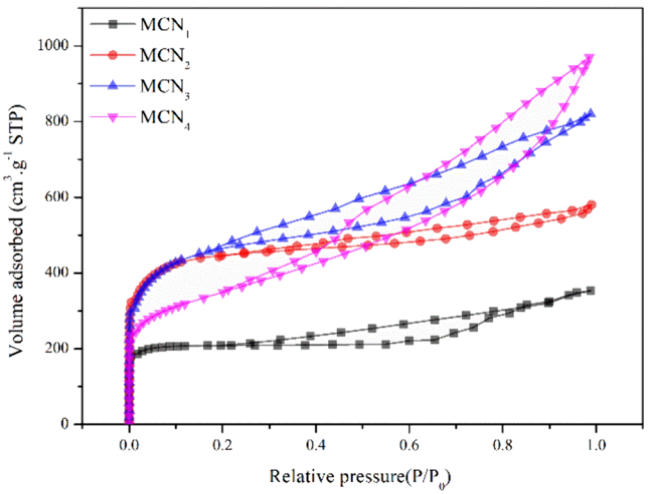

Figure 2. N_2 adsorption−desorption isotherms of MCN_1, MCN_2, MCN_3, and MCN_4.

Table 1. Structural Parameters of Mesoporous Carbon

samples	S_{BET} (m^2/g)	V_{total} (cm^3/g)	V_{mic} (cm^3/g)	V_{meso} (cm^3/g)	D_{BJH} (nm)
MCN_1	648.372	0.546	0.3206	0.2254	3.366
MCN_2	1197.054	0.897	0.6631	0.2339	2.558
MCN_3	1403.363	1.268	0.6715	0.5965	3.343
MCN_4	1517.485	1.501	0.4929	1.0081	5.017

diffusion channel for heavy metal ions. The highest contact region may be present in MCN_4 due to its largest surface area.

To compare the surface chemical compositions between MCN_1, MCN_2, MCN_3, and MCN_4, we conducted a thorough investigation of the types and quantities of functional groups using XPS. Figure 3a shows the binding energy spectrum of carbon, oxygen, nitrogen, and sulfur atoms of the samples. The spectra of all samples show that MCN_1 consisted of C 1s (285 eV), O 1s (532 eV), and N 1s (400.0 eV).[40] MCN_2 and MCN_3 show the presence of C (1s), O (1s), and S (2s, 2p) peaks in Figure 3a, while MCN_4 contains the C (1s) and the O (1s), attributed to the degradation of ammonium thiosulfate. The total carbon contents in MCN_1, MCN_2, MCN_3, and MCN_4 are 83.22, 89.72, 91, and 84.24% respectively. It suggests that the carbon content of MCNs is related to the carbonization temperature. The MCN oxygen contents are 9.7, 7.92, 7.31, and 13.13%. MCN_4 has the highest oxygen content, ascribed to being oxidized by nitric acid. The quantitative analysis of the sample surface functionalities is shown in Table 2. High-resolution core spectra of C 1s are shown in Figure 3b−e. The C 1s band of MCN_1 included Three peaks centered at 284.7, 285.7, and 288.8 eV, attributed to sp^2 carbon, sp^3carbon, and carbonyl groups (O−C═O, N−C═O), respectively.[41,42] The existence of elements O and N to provide extra active sites in MCN_1 is essential to enhance the chelating ability of MCN_1.[38] The peak at 287.1 eV of MCN_2 is typical of carbon atoms bound to one oxygen with a double bond (C═O).[38,40,43] By comparing MCN_2 and MCN_3, the sp^2C contents range from 73.12 to 56.7%, indicating that sp^2C contents decrease with increasing carbonization temperature. MCN_2, MCN_3, and MCN_4 contain oxygen-containing functionalized groups. Therefore, samples prepared by different methods have varying carbon and chemical compositions, which can provide a broader range of active sites for mercury adsorption.

XRD patterns of MCN_1, MCN_2, MCN_3, and MCN_4 can be seen in Figure 4. MCNs from different carbonization periods and templates exhibit diffraction peaks(2θ = 25.3°, 43.5°) that correspond with amorphous carbon's (002) and (101) peaks.[44−47] The d_{002} values of MCN_1, MCN_2, MCN_3, and MCN_4 are 3.55 3.70, 3.71, and 3.53 Å, respectively. The d002 values of all samples are larger than that of graphite (3.35 Å), indicating that they all have an amorphous structure. During the carbonization process, active groups (from both soft and hard templates) become mobile, resulting in the formation of dense aromatic compounds. Additionally, the coking process generates further carbon under high temperatures. As a consequence, amorphous carbon within MCNs exhibits characteristic diffraction patterns due to the presence of aromatic layers.

2.2. Adsorption Studies. Based on the preferential adsorption results for MCN_1, MCN_2, MCN_3, and MCN_4 for Pb(II), As(II), Cd(II), Hg(II), and Cu(II), as shown in Table S1, MCNs synthesized by different template methods all show certain selective removal performance for Hg(II), and the selective removal rate of Hg(II) by MCN_1 is as high as 92.18%. Figure S2 illustrates the influence of the adsorbent dosage on the efficiency of Hg(II) removal. Balancing both removal efficiency and cost-effectiveness, 5.0 mg was deemed the optimal dosage for subsequent experiments pertaining to the adsorption of low-concentration Hg(II). Figure S3 demonstrates the impact of varying initial concentrations on Hg(II) adsorption. Considering the significant removal rate achieved, it was determined that 20 mg·L^{-1} was the optimal concentration for the Hg(II) solution. To investigate factors affecting the adsorption performance and mechanism of the samples, experiments were conducted under controlled conditions on the following samples (MCN_1, MCN_2, MCN_3, and MCN_4), using an optimal dosage of 5.0 mg and an initial Hg(II) concentration of 20 mg·L^{-1}.

2.2.1. Effects of Initial pH on Adsorption. Varying the pH level of a solution modifies not only the surface charge and functional groups of the adsorbent but also the existing form of Hg(II). In particular, when the concentration of Hg(II) in a 20 mL solution is set to 10.0 mg·L^{-1}, the pH threshold at which mercury ions start to precipitate is approximately 9.8.[34] The pH range of this experiment is therefore 2.0−9.0. The removal efficiencies of Hg(II) on MCN_1, MCN_2, MCN_3, and MCN_4 remained consistently high, exceeding 90.0%, across a range of pH conditions from 2.0 to 9.0, with minimal variations (Figure 5). Due to the oxygen-containing and nitrogen-containing functional groups in MCN_1, MCN_2 (which contained oxygen-functional groups such as hydroxyl and carboxyl), and MCN_4, these groups served as active sites for Hg(II) complexation.[4,44] However, the presence of Hg(II) significantly first increased and then decreased with increasing pH(pH at 2.0−9.0) for MCN_3, which may be due to the surface −COO of MCN_3 and the change in zeta potential (Figure S5).[4] It has shown significant potential to remove Hg(II) from real wastewater over a wide pH range. Honeysuckle decoction is usually a traditional Chinese medicine (TCM) or food. Given the neutral characteristics of the honeysuckle decoction, a pH value of 7.0 was selected as the most effective condition for the removal of Hg(II) from the herbal mixture.

2.2.2. Adsorption Kinetics. The adsorption kinetics of MCNs are described by the pseudo-first-order (eq 1), and the pseudo-second-order (eq 2).[48]

https://doi.org/10.1021/acsomega.4c03269
ACS Omega 2024, 9, 44931−44941

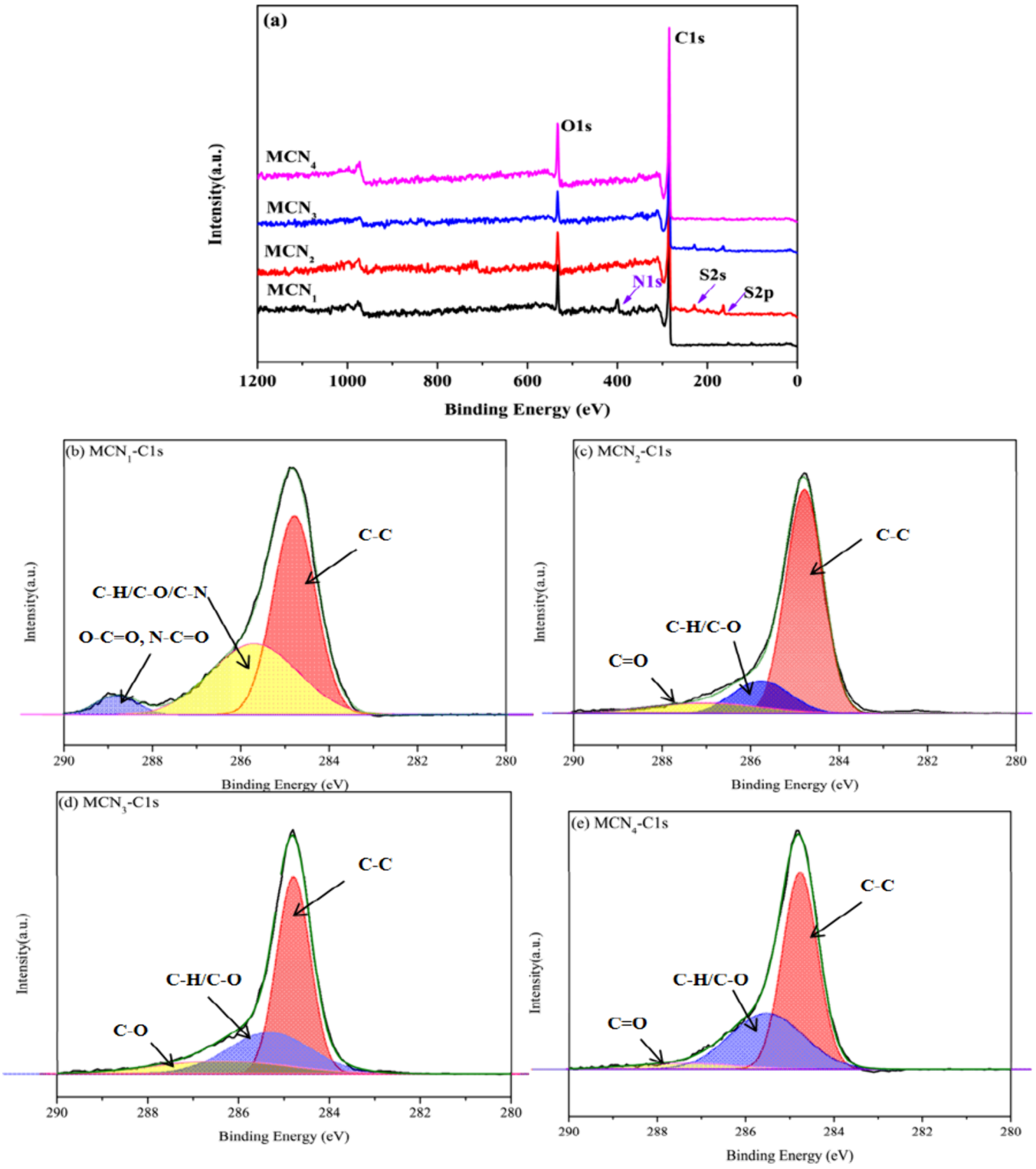

Figure 3. Overall XPS scan of the MCN_1, MCN_2, MCN_3, and MCN_4 (a), C-1s peak analysis of MCN_1 (b), MCN_2 (c), MCN_3 (d) and MCN_4 (e).

$$\log(Q_e - Q_t) = \log Q_e - \frac{k_1 t}{2.303} \quad (1)$$

$$\frac{t}{Q_t} = \frac{1}{q} Q_e{}^2 k_2 + \frac{t}{Q_e} \quad (2)$$

The pseudo-first-order rate constant is designated as $k_1(\text{min}^{-1})$, while the pseudo-second-order sorption rate constant is represented by k_2 $(\text{g}\cdot(\text{mg}\cdot\text{min})^{-1})$. At a specific time t (min), the adsorbed quantity of mercury ions is denoted as Q_t $(\text{mg}\cdot\text{g}^{-1})$, and the equilibrium sorption capacity is referred to as Q_e $(\text{mg}\cdot\text{g}^{-1})$. Notably, in this work, MCNs were considered to be spherical in shape. Detailed results derived from the application of kinetic models to the experimental data are presented in Figure 6 and Table 3.

As indicated in Table 3, the four pseudo-second-order kinetic models exhibited correlation coefficients of R^2 exceed-

https://doi.org/10.1021/acsomega.4c03269
ACS Omega 2024, 9, 44931−44941

Table 2. Contents of MCNs Obtained from the Fitting Results of the C 1s Spectrum

samples	peaks	binding energy (eV)	oxygen form	atomic ratio (%)
MCN_1	1	284.7	sp^2C	54.68
	2	285.7	C−H/C−O/C−N	39.70
	3	288.8	O−C═O, N−C═O	5.32
MCN_2	1	284.8	sp^2C	73.12
	2	285.8	C−H/C−O	16.26
	3	287.1	C═O	10.62
MCN_3	1	284.8	sp^2C	56.70
	2	285.3	C−H/C−O	29.04
	3	286.4	C−O	14.25
MCN_4	1	284.8	sp^2C	59.36
	2	285.5	C−H/C−O	35.34
	3	287.4	C═O	5.29

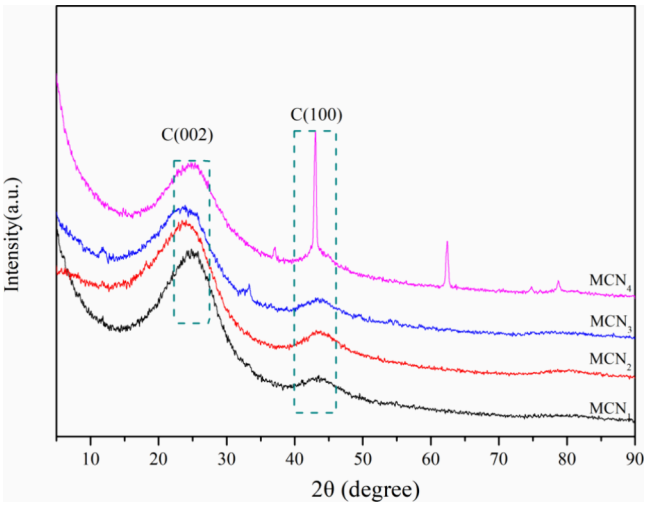

Figure 4. XRD patterns of MCN_1, MCN_2, MCN_3, and MCN_4.

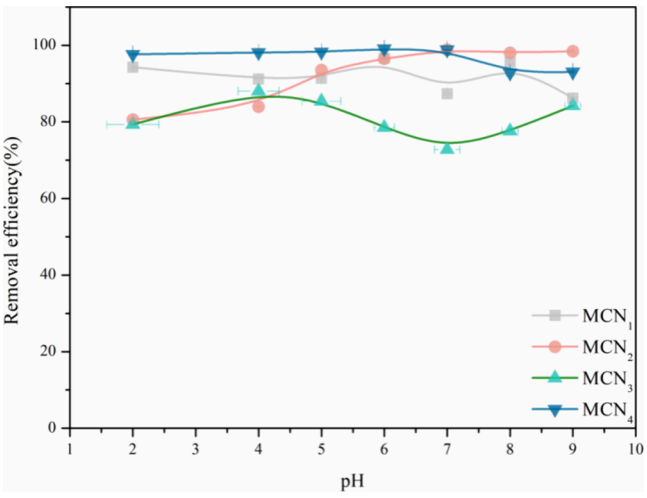

Figure 5. Removal rate of MCNx for mercury ions at different pH values.

ing 0.999, surpassing those of the pseudo-first-order models. Furthermore, the Q_e values calculated using the pseudo-second-order equation aligned more closely with the actual adsorption quantities, suggesting that the Hg(II) adsorption mechanisms of MCNs may be more accurately described by the pseudo-second-order kinetic models. This provides evidence that the adsorption process is primarily influenced by chemisorption.[4] The kinetic constant (k_2) of MCN_1 and MCN_2 is calculated to be near 0.30 g·(mg· min)$^{-1}$, due to the rational design of the hierarchical structure.[5]

2.2.3. Adsorption Isotherm. 5.0 mg of MCNs was diluted to 20 mL of different concentrations in this study (0.01, 0.13, 0.16, 0.19, 0.22, 0.30, and 0.40 mg·L^{-1}) in Hg(II) for adsorption experiments. Adsorption results are shown in Figure S4. To explore the adsorption mechanism of Hg(II) onto MCNs, both the Freundlich (eq 3) and Langmuir adsorption models (eq 4)[48] were employed for equilibrium data analysis.

$$\frac{C_e}{Q_e} = \frac{1}{Q_{max}K_L} + \frac{C_e}{Q_{max}} \tag{3}$$

$$\ln Q_e = \frac{1}{n}\ln C_e + \ln K_F \tag{4}$$

In analyzing the adsorption mechanism of Hg(II) onto MCNs, we utilized the Freundlich and Langmuir adsorption models. Here, C_e(mg·L^{-1}) signifies the equilibrium concentration of Hg(II), while Q_e(mg·g^{-1}) represents the adsorbed amount of Hg(II) at equilibrium. Q_{max} (mg·g^{-1}) denotes the maximum adsorption capacity of MCNX, and K_L (L·mg^{-1}) is a Langmuir constant reflecting the surface adsorption energy. K_F (mg·g^{-1})(L·mg^{-1})$^{1/n}$, on the other hand, represents the Freundlich constants associated with sorption capacity, and n indicates the sorption intensity. For a detailed view of the fitting curve and parameters, refer to Figure 7 and Table 4.

As is evident from Table 4, the Freundlich isotherm model provides a more accurate description of Hg(II) adsorption by MCNs when comparing the correlation coefficients (R^2) of both models. However, Freundlich models offer a superior simulation of trace metal adsorption on all MCNs, suggesting a unimolecular layer adsorption mechanism during the adsorption process of MCNs.[48] The Freundlich constant (n) exceeded 1 for MCN_1, MCN_2, and MCN_4, suggesting that the adsorption of Hg(II) onto MCN_1, MCN_2, and MCN_4 was favorable and preferential.[48] Further evidence supports the occurrence of chemical adsorption.

2.3. Performances In Situ Removal of Mercury in Honeysuckle. In this study, we measured the Hg(II) concentration in honeysuckle samples obtained from the laboratory. Our findings revealed the presence of a trace amount of mercury, with a concentration ranging from approximately 0.005−0.013 mg·kg^{-1}. Therefore, under the optimal conditions, MCNs were used for in situ adsorption of Hg(II) of honeysuckle water decoction, and the results are demonstrated in Figure 8. As observed in Figure 8, the in situ Hg(II) removal efficiencies of MCN_1, MCN_2, MCN_3, and MCN_4 were 80, 56, 38, and 57%, respectively. Compared to the Hg(II) solution, MCNs exhibit lower removal efficiency for in situ Hg(II) from honeysuckle water decoctions. This suggests that the decoction itself contains components that occupy the active adsorption sites on mesoporous carbon. Additionally, the ultralow concentration of Hg(II) and limited contact sites may contribute to the difficulty in adsorption, resulting in reduced adsorption efficiency. Notably, MCN_1 demonstrates a higher removal efficiency compared to those of MCN_2, MCN_3, and MCN_4, potentially due to its increased number of adsorption sites or chelating groups.

https://doi.org/10.1021/acsomega.4c03269
ACS Omega 2024, 9, 44931−44941

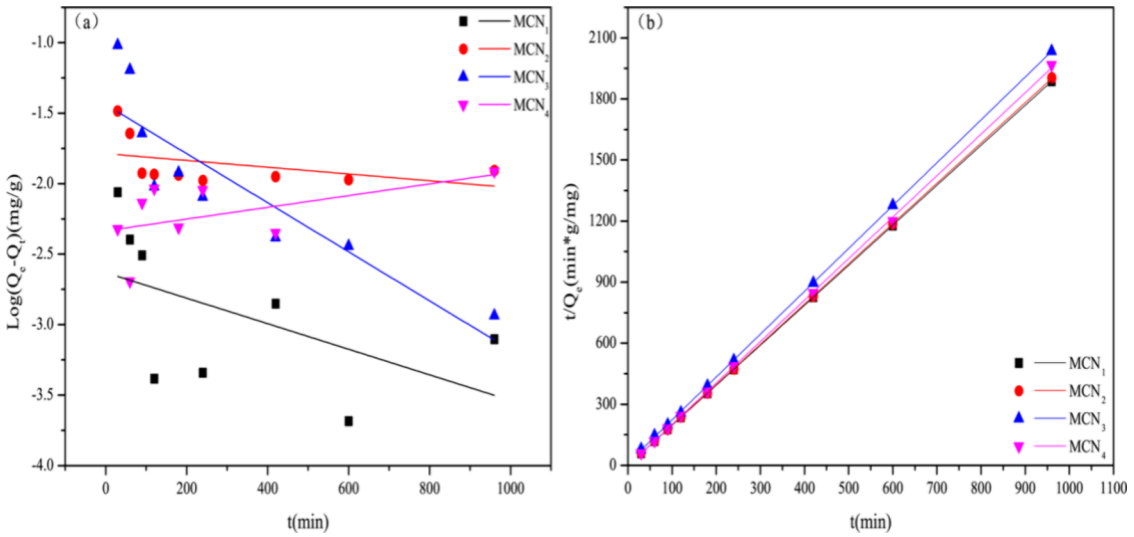

Figure 6. Line kinetic plot for the Hg(II) adsorption via the pseudo-first-order model and the pseudo-second-order model for MCNs: (a) pseudo-first-order model; (b) pseudo-second-order model.

Table 3. Kinetic Parameters of the Pseudo-Second-Order and the Pseudo-First-Order Models of MCNs for Hg(II)

		pseudo-first-order			pseudo-second-order		
kinetic models	$q_{e\exp}$ (mg/g)	Q_e (mg/g)	K_1 (1/min)	R^2	q_e (mg/g)	K_2 (g/(mg·min))	R^2
MCN_1	0.5094	0.0023	6.058	0.1599	0.5088	0.3034	0.99999
MCN_2	0.5169	0.0163	4.1168	0.0672	0.5052	0.3499	0.99999
MCN_3	0.4730	0.0363	3.3159	0.7493	0.4749	9.0147	0.99996
MCN_4	0.5002	0.0046	5.37612	0.1473	0.4907	2.3255	0.99976

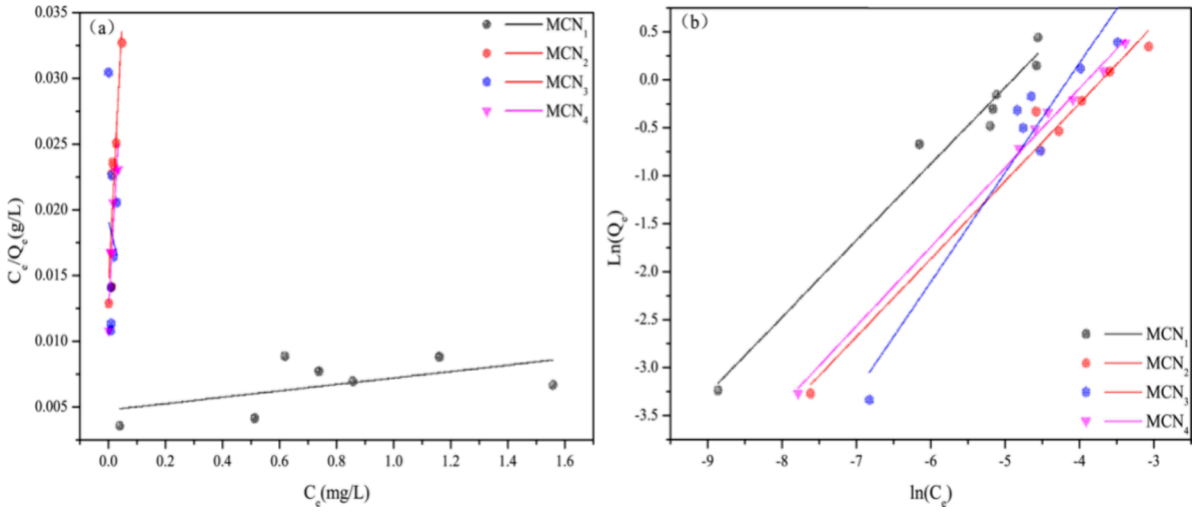

Figure 7. Langmuir and Freundich isotherm Equation simulation curve of MCNs: (a) Langmuir and (b) Freundich.

Table 4. Parameters for the Langmuir and the Freundlich models of MCN_1, MCN_2, MCN_3 and MCN_4 for Hg(II)

	Langmuir model			Freundlich model		
samples	Q_{max} (mg/g)	K_L (L/mg)	R^2	K_F (mg/g) $(L/mg)^{1/n}$	n	R^2
MCN_1	411.5226	0.000011	0.1764	50.0830	1.2529	0.9704
MCN_2	2.4450	0.0060	0.7708	20.2056	1.2316	0.9729
MCN_3	−11.7096	0.0016	0.1842	115.3972	0.8753	0.9058
MCN_4	2.7581	0.0046	0.8572	25.0642	1.2091	0.9960

2.4. Analysis of Chlorogenic Acid Content of HPLC Index Medicinal Component. In the "Pharmacopoeia of the People's Republic of China" (2020 edition), chlorogenic acid is listed as one of the indexes containing the honeysuckle extract. To evaluate the impact of mesoporous carbon on chlorogenic acid in honeysuckle water decoctions during

https://doi.org/10.1021/acsomega.4c03269
ACS Omega 2024, 9, 44931−44941

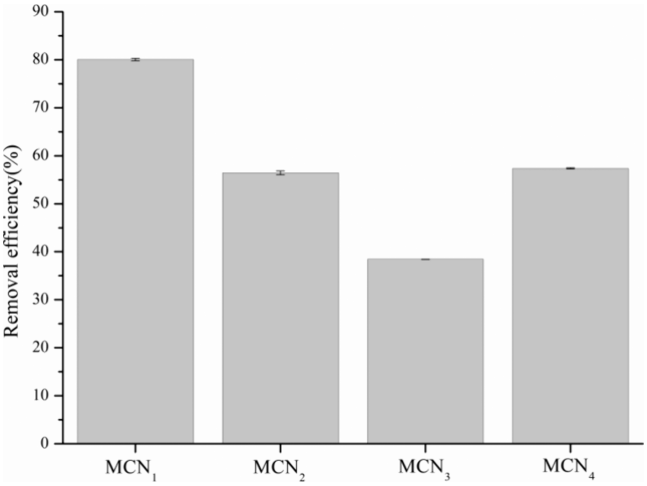

Figure 8. Removal efficiency of mesoporous carbon against in situ Hg(II) from Honeysuckle water decoction.

Hg(II) removal, we undertook a comparative analysis of the chlorogenic acid peak areas. In this study, the peak areas of chlorogenic acid were compared among standard solutions, untreated lonicerae decoction, and aqueous decoction treated with mesoporous carbon MCNs to determine the difference in the peak areas of chlorogenic acid, which is a medicinal component. A summary of the results can be found in Figure 9

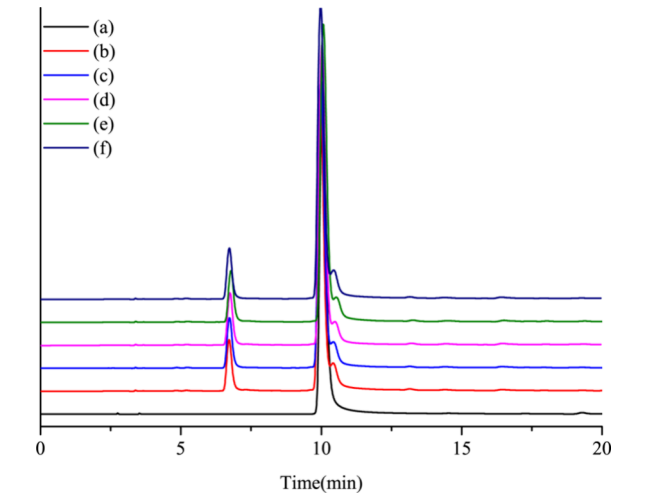

Figure 9. HPLC diagrams: (a) chlorogenic acid standard, (b) honeysuckle water decoction, (c) honeysuckle water decoction after Hg(II) removal by MCN_1, (d) honeysuckle water decoction after Hg(II) removal by MCN_2, (e) honeysuckle water decoction after Hg(II) removal by MCN_3, and (f) honeysuckle water decoction after Hg(II) removal by MCN_4.

The retention time of chlorogenic acid in the standard solution (a) was 10.044 min, and the retention time of chlorogenic acid in the honeysuckle water decoction (b) was 9.968 min. The retention times of chlorogenic acid in the honeysuckle water decoctions after Hg(II) removal from MCN_1 (c), MCN_2 (d), MCN_3 (e), and MCN_4 (f) were 9.984, 10.023, 10.072, and 9.978 min, respectively.

The peak areas of chlorogenic acid were 22282.5, 22326.2, 23186.8, 23203.4, and 22581.1 mAu·min. The peak area and retention time of the chlorogenic acid were nearly identical. The relative standard deviation of peak area (RSD%) was 1.78. Based on these findings, it can be concluded that mesoporous carbon MCNs have a minimal impact on the adsorption of chlorogenic acid.

2.5. Adsorption Mechanism. Since MCN_2, MCN_3, and MCN_4 have roughly equivalent adsorption rates for Hg(II) in honeysuckle decoction, MCN_1 and MCN_2 were selected for adsorption mechanism studies. The adsorption mechanism of Hg(II) by MCNs was investigated by using XPS. XPS survey spectra (Figure 10a) revealed that new peaks associated with Hg 4f core-level signals appeared for both MCN_1 and MCN_2 after Hg(II) adsorption. As evident from the high-resolution figure of Hg (Figure 10b,c), the intensity of the Hg 4f5/2 peak at 101.71 eV after adsorption with MCN_1 is substantially higher than that of MCN_2, indicating that MCN_1 has a stronger adsorption capacity for Hg(II). Based on the XPS results, MCN_1 exhibits a strong affinity for Hg(II) complexes, which can be explained by its excellent Hg(II) complexation ability. These data confirm that Hg(II) was successfully immobilized on MCN_1 through adsorption.

3. CONCLUSIONS

In conclusion, a range of oxygen- and nitrogen-containing functional mesoporous carbons have been synthesized through the pyrolysis of various carbon sources. Specifically, mesoporous carbon with N-functionality (MCN_1) was successfully synthesized using melamine as the carbon and nitrogen source, with the triblock copolymer F127 serving as the soft template agent. Additionally, oxygen-functional mesoporous carbon materials (MCNs) were effectively synthesized using sucrose as the carbon source and subsequently oxidized with concentrated nitric acid. Results show that MCN_1, MCN_2, MCN_3, and MCN_4 have a micro- and mesoporous structure on the surface and inside. MCN_1 exhibited a specific surface area of 648.372 $m^2 \cdot g^{-1}$. The specific surface areas of MCN_2, MCN_3, and MCN_4 respectively correspond to 1197.054, 1403.363, and 1517.485 $m^2 \cdot g^{-1}$. The approximate D_{BJH} of MCN_1 and MCN_4 is around 3.3 nm. All of the materials are present in the form of amorphous carbon.

Analysis of adsorption experiments demonstrated that MCN_1 has the highest removal efficiency of 80% for trace mercury(Hg) in honeysuckle decoction, exceeding the highest removal efficiency achieved in previous studies by 14% (Table 5).[34] MCN_2 and MCN_4 have similar removal efficiencies of 56 and 57% for trace mercury in honeysuckle decoction. Adsorption mechanism results show that the removal efficiency of trace mercury benefits from chelation interactions between Hg(II) and nitrogen binding, as well as the ion diffusion channel in the mesoporous pore. Such superior features of MCN_1 make it a very good candidate for deep removal of Hg(II) from honeysuckle decoction in practical applications. This work presents a new approach to an effective adsorbent for removing trace mercury(Hg) in complex Chinese herbal medicine decoctions.

4. MATERIALS AND METHODS

4.1. Materials. Formaldehyde(37 wt %), phenol, hydrochloric acid, nitric acid, melamine, and ammonium thiosulfate were purchased from Shanghai Energy Chemical Co., Ltd. (China). Pluronic acid F127 was obtained from Sigma-Aldrich Co., Ltd. Nano magnesium oxide was purchased from Shanghai Macklin Biochemical Co., Ltd. (China). The chlorogenic acid standard was bought from Beijing Solarbio

https://doi.org/10.1021/acsomega.4c03269
ACS Omega 2024, 9, 44931−44941

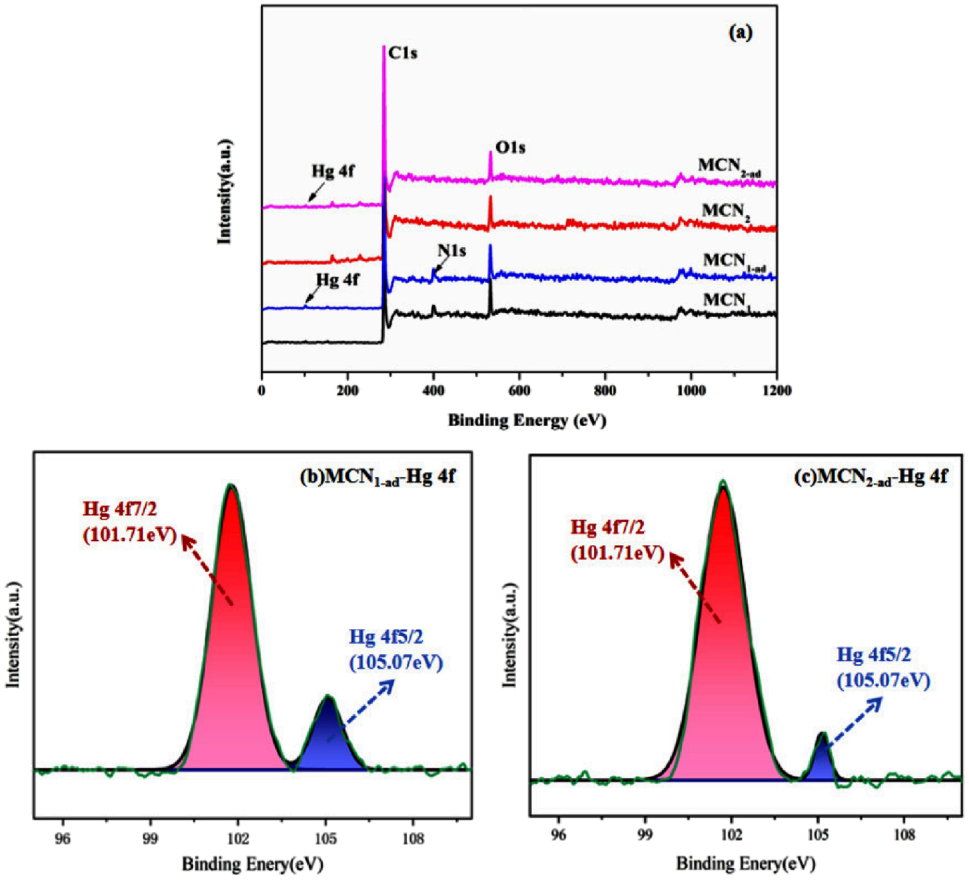

Figure 10. Overall XPS scan of the MCN_1, $MCN_{1\text{-}ad}$, MCN_2, and $MCN_{2\text{-}ad}$ (a), Hg 4f peak analysis of $MCN_{1\text{-}ad}$ (b) and $MCN_{2\text{-}ad}$ (c).

Table 5. Comparison of Removal Rates of Hg(II) In Situ from Aqueous Decoction of Honeysuckle

samples	removal (%)
MCN_1	80
PC-2[34]	66

Technology Co. Ltd., China. The content of mercury (0.009−0.011 $mg{\cdot}kg^{-1}$) in Honeysuckle was tested by the Guizhou Institute of Products Quality Inspection & Testing, Guiyang, China. The detection of Honeysuckle mercury content has been explained in detail elsewhere.[34] A mercury standard solution(1000 $\mu g{\cdot}mL^{-1}$) was purchased from the National Nonferrous Metal and Electronic Materials Analysis and Testing Center, China.

4.2. Fabrication and Characterization of MCN_X. In this study, the MCN_X was obtained from the simple pyrolysis process described in a previous study.[34] This work builds on our prior research to tailor mesoporous carbon in order to better control the final structure of the mesoporous carbon, thereby enhancing the removability of trace mercury from Honeysuckle water decoction. The optimal fabrication methods are as follows.

4.2.1. Fabrication of MCN_1. A 1.798 g portion of melamine, 2.1 mL of 37% formaldehyde solution, and 15.0 mL of deionized water were mixed at 80 °C in a flask. Separately, a solution was prepared by combining 0.6 g of phenol, 2.1 mL of a 37% formaldehyde solution, and 15.0 mL of sodium hydroxide. This mixture was stirred for 30 min at 66 °C. Pluronic F127 was dissolved in 15.0 mL of deionized water and gradually added to the previous mixture after stirring for 2 h at 66 °C. Subsequently, 15.0 mL of deionized water was added to the combined solution. It was observed that the reaction mixture turned cloudy and formed precipitates after approximately 20 h, at which point the experiment was terminated. Subsequently, the solution was placed in a hydrothermal reactor and heated to 130 °C for 24 h, followed by cooling to room temperature. The upper solid layer was then calcined at 800 °C for 3 h with a heating rate of 5 °C/min under a nitrogen flow. Finally, the sample was washed with distilled water, neutralized, and dried (Figure S1). This prepared sample is designated as MCN_1.

4.2.2. Fabrication of MCNx. Sucrose and concentrated nitric acid are evenly mixed in a specific ratio and placed for about 2−3 days, then heated to 160 °C for 2−3 h, cooled to room temperature, and ground, and a carbonaceous precursor is obtained. The carbonaceous precursor was then mixed with 1/2 sucrose, ammonium sulfate, and nanomagnesium oxide. After the mixture was thoroughly mixed, it was carbonized under a nitrogen atmosphere for 2 h at 800 °C at a rate of 5 $°C{\cdot}min^{-1}$. Finally, the sample was washed with distilled water and dried. The obtained sample was denoted as MCN_2. With other conditions unchanged, the calcination temperature was increased from 800 to 900 °C for 2 h to further remove the template agent, and the prepared material was named MCN_3. Keeping other conditions kept unchanged, MCN_2 was refluxed in an ethanol-hydrochloric acid solution and oxidized by nitric acid to obtain MCN_4.

4.3. Characterization. Mesoporous carbon morphologies were examined using scanning electron microscopy (SEM,

https://doi.org/10.1021/acsomega.4c03269
ACS Omega 2024, 9, 44931−44941

Zeiss-Sigma300, Zeiss, Germany) and transmission electron microscopy (TEM, Axio Scope AI A, Zeiss, Germany). The chemical constitution of mesoporous carbon was analyzed by an X-ray photoelectron spectrometer (XPS, ESCALAB Xi$^+$, Thermo Scientific, USA). The surface potential of mesoporous carbon was analyzed by a zeta potential analyzer (NanoBrook 90plus PALS). The specific surface area and pore structure of samples were identified by specific surface area and porosity analyzer (JW-BK122W, Beijing, China), which were determined by the Brunauer−Emmett−Teller method using nitrogen as the adsorbate at 77 K. The crystallography of mesoporous carbon was conducted by X-ray diffraction (XRD, X'Pert Powder, Panalytical, Netherlands) with Cu Kα radiation (λ = 0.15406 nm).

4.4. Adsorption Studies. Hg(II) adsorption experiments were performed at various pHs, adsorption times, and temperatures using different concentrations of Hg(II) and the adsorbent. Prior to the analysis of residual heavy metal concentrations, all samples were filtered with 0.22 μm membrane filters. The Hg(II) concentrations were measured using an inductively coupled plasma mass spectrometer(ICP-MS, iCAP6300MFC, Thermo Fisher, USA). The removal efficiency (E) of Hg(II) is calculated as follows[5,33]:

$$E(\%) = \frac{(C_0 - C_e)}{C_0} \times 100\% \quad (5)$$

where C_0 (mg·L^{-1}) and C_e(mg·L^{-1}) are the initial concentration and adsorption equilibrium concentration of Hg(II), respectively.

Hg (II) equilibrium adsorption amount is calculated as follows[5,33]:

$$Q_e = \frac{(C_0 - C_e)}{m} \times V \quad (6)$$

where Q_e(mg·g^{-1}) is the equilibrium adsorption capacity of Hg(II); C_0 (mg·L^{-1}) is the initial concentration of Hg(II); C_e (mg·L^{-1}) is the adsorption equilibrium concentration of Hg(II); and V (mL) and m (g) are the object volume of Hg(II) and the amount of adsorbent. Adsorption kinetics, thermodynamics, and isotherms were all studied under optimal conditions.

4.5. Removal of Hg(II) from Honeysuckle Water Decoction. This process has been well documented in our previous work.[34] The honeysuckle powder (1.00 g) was diluted in deionized water and extracted for 30 min. After filtering, deionized water was added to confirm the concentration and to clarify the water decoction. Subsequently, 5.00 mg of MCNs were introduced into 20 mL of honeysuckle water decoction and agitated at 30 °C for 30 min while maintaining all other conditions constant. The resulting mixtures were then separated, and the samples were analyzed by using ICP-MS to determine the removal efficiency. All of the experiments were performed at least three times.

4.6. Effect of MCNs on the Pharmacodynamic Component of Honeysuckle Decoction. MCNs were blended with honeysuckle decoction for 30 min at 30 °C. Subsequently, the mixtures were filtered and submitted for high-performance liquid chromatography (HPLC) analysis. HPLC (Agilent 1260, USA) was employed to assess the impact of MCNs on the active ingredient, chlorogenic acid, in honeysuckle. The chlorogenic acid standard was dissolved in 50% methanol to prepare standards (0.0535 mg·mL^{-1}). The chromatographic conditions were set as follows: a ZORBAX SB-C18 column (4.6 × 250 mm, 5 μm) was used, maintained at room temperature. The mobile phase consisted of acetonitrile and 0.5% glacial acetic acid with a flow rate of 1.0 mL·min^{-1} and a detection wavelength of 326 nm.

■ ASSOCIATED CONTENT

Supporting Information

The Supporting Information is available free of charge at https://pubs.acs.org/doi/10.1021/acsomega.4c03269.

Schematic diagram for mesoporous carbon synthesis and in situ adsorption of mercury ions; research on selective removal of heavy metals by mesoporous carbon(DOC); investigation of the impact of mesoporous carbon dosage on Hg(II) removal efficiency; examination of Hg(II) concentration on the removal efficiency for mesoporous carbon; analysis of the effect of temperature on Hg(II) removal; and exploration of the influence of pH on zeta potential (PDF)

■ AUTHOR INFORMATION

Corresponding Authors

Jianyong Zhang − *School of Pharmacy, Zunyi Medical University, Zunyi 563000, China*; Email: zhangjianyong2006@126.com

Ming Yu − *School of Pharmacy, Zunyi Medical University, Zunyi 563000, China; State Key Laboratory of Natural and Biomimetic Drugs, School of Pharmaceutical Sciences, Peking University, Beijing 100191, China*; orcid.org/0000-0001-5060-4249; Email: Cosmosym920@163.com

Authors

Qing He − *School of Pharmacy, Zunyi Medical University, Zunyi 563000, China*

Kun Pang − *School of Pharmacy, Zunyi Medical University, Zunyi 563000, China*

Lin Tian − *School of Pharmacy, Zunyi Medical University, Zunyi 563000, China*

Yiqian Ma − *Guizhou Institute of Products Quality Inspection & Testing, Guiyang 550025, China*

Xiang Guo − *School of Pharmacy, Zunyi Medical University, Zunyi 563000, China*

Complete contact information is available at: https://pubs.acs.org/10.1021/acsomega.4c03269

Notes

The authors declare no competing financial interest.

■ ACKNOWLEDGMENTS

This study was supported by Natural Science Foundation of Guizhou Province China (Basic of Guizhou Science and Technology Basic-ZK [2022] General 617), Doctoral StartUp Foundation of Zunyi Medical University (Guizhou Science and Technology branch [2018]5772-034), National College Student Innovation and Entrepreneurship Plan Project of China (no. ZYDC2022016 and no. ZYDC2022025).

■ REFERENCES

(1) Zuo, T. T.; Jin, H. Y.; Zhang, L.; Liu, Y. L.; Nie, J.; Chen, B. L.; Fang, C. F.; Xue, J.; Bi, X. Y.; Zhou, L.; Shen, M. R.; Shi, S. M.; Ma, S. C. Innovative health risk assessment of heavy metals in Chinese herbal

medicines based on extensive data. *Pharmacol. Res.* **2021**, *163*, No. 105268.
(2) Yang, C. M.; Chien, M. Y.; Chao, P. C.; Huang, C. M.; Chen, C. H. Investigation of toxic heavy metals content and estimation of potential health risks in Chinese herbal medicine. *J. Hazard Mater.* **2021**, *412*, No. 125142.
(3) Renu, K.; Chakraborty, R.; Myakala, H.; Koti, R.; Famurewa, A. C.; Madhyastha, H.; Vellingiri, B.; George, A.; Valsala Gopalakrishnan, A. Molecular mechanism of heavy metals (Lead, Chromium, Arsenic, Mercury, Nickel and Cadmium) - induced hepatotoxicity - A review. *Chemosphere* **2021**, *271*, No. 129735.
(4) Bao, S.; Wang, Y.; Wei, Z.; Yang, W.; Yu, Y.; Sun, Y. Amino-assisted AHMT anchored on graphene oxide as high performance adsorbent for efficient removal of Cr(VI) and Hg(II) from aqueous solutions under wide pH range. *J. Hazard Mater.* **2021**, *416*, No. 125825.
(5) Gutiérrez, I. S.; Morales, V. H.; Muñoz, E.; Mendoza, R. N.; Soto, L. L.; Ledesma, C.; Casados, D. S.; Pawelec, B. Efficient Removal of Hg(II) from Water under Mildly Acidic Conditions with Hierarchical SiO2Monoliths Functionalized with -SH Groups. *Materials (Basel)* **2022**, *15* (4), 1580.
(6) Jun, L. I.; Chuanwu, F. U.; Juanyong, L. I. Determination of Five Heavy Metals in Zhuang-drug Millettia pulchra Kurz var. Laxior-(Dunn) Z. Wei by Inductively Coupled Plasma Mass Spectrometry with the Microwave Digestion. *Chin. J. Drug Eval.* **2016**, *7* (1), 126.
(7) Zuo, T. T.; Zhang, L.; Wang, Y.; Nie, L. X.; Shen, M. R.; Liu, L. N.; Yu, J. D.; Jin, H. Y.; Wei, F.; Ma, S. C. Technical guidelines for risk assessment of heavy metals in traditional Chinese medicines. *Chin. Med.* **2023**, *18* (1), 69.
(8) Chen, W.; Yang, Y.; Fu, K.; Zhang, D.; Wang, Z. Progress in ICP-MS Analysis of Minerals and Heavy Metals in Traditional Medicine. *Front Pharmacol* **2022**, *13*, No. 891273.
(9) Yao, T.; Jiang, S.; Hou, K.; Sun, H.; Wang, H. Cadmium (Cd) accumulation in traditional Chinese medicine materials (TCMMs): A critical review. *Ecotoxicol Environ. Saf* **2022**, *242*, No. 113904.
(10) Chen, Y.; Zou, J.; Sun, H.; Qin, J.; Yang, J. Metals in Traditional Chinese medicinal materials (TCMM): A systematic review. *Ecotoxicol Environ. Saf* **2021**, *207*, No. 111311.
(11) Ma, H.; Wu, L. M.; Zou, Y.; Li, X. A. Non-occupational lead poisoning associated with traditional Chinese medicine: A case report. *Front Public Health* **2022**, *10*, No. 938186.
(12) Ernst, E. Toxic heavy metals and undeclared drugs in Asian herbal medicines. *Trends Pharmacol. Sci.* **2002**, *23* (3), 136−139.
(13) Meng, C.; Wang, P.; Hao, Z.; Gao, Z.; Li, Q.; Gao, H.; Liu, Y.; Li, Q.; Wang, Q.; Feng, F. Ecological and health risk assessment of heavy metals in soil and Chinese herbal medicines. *Environ. Geochem Health* **2022**, *44* (3), 817−828.
(14) Ma, X.; Hua, M. Z.; Ji, C.; Zhang, J.; Shi, R.; Xiao, Y.; Liu, X.; He, X.; Zheng, W.; Lu, X. Rapid screening and quantification of heavy metals in traditional Chinese herbal medicines using monochromatic excitation energy dispersive X-ray fluorescence spectrometry. *Analyst* **2022**, *147* (16), 3628−3633.
(15) Guo, L.; Qiao, J.; Zhang, L.; Yan, W.; Zhang, M.; Lu, Y.; Wang, Y.; Ma, H.; Liu, Y.; Zhang, Y.; Li, J.; Qin, D.; Huo, J. Critical review on anthocyanins in blue honeysuckle (Lonicera caerulea L.) and their function. *Plant Physiol Biochem* **2023**, *204*, No. 108090.
(16) Jurikova, T.; Rop, O.; Mlcek, J.; Sochor, J.; Balla, S.; Szekeres, L.; Hegedusova, A.; Hubalek, J.; Adam, V.; Kizek, R. Phenolic profile of edible honeysuckle berries (genus lonicera) and their biological effects. *Molecules* **2012**, *17* (1), 61−79.
(17) Golubev, D.; Zemskaya, N.; Shevchenko, O.; Shaposhnikov, M.; Kukuman, D.; Patov, S.; Punegov, V.; Moskalev, A. Honeysuckle extract (Lonicera pallasii L.) exerts antioxidant properties and extends the lifespan and healthspan of Drosophila melanogaster. *Biogerontology* **2022**, *23* (2), 215−235.
(18) Bu, T.; Yu, X.; Zhang, X. R.; Li, J.; Wang, L. N.; Zhang, F.; Zhang, Y. Q. Analysis of heavy metal pollution in Lonicerae Japonicae Flos and its health risk assessment. *Zhongguo Zhong Yao Za Zhi* **2022**, *47* (3), 643−650.
(19) Kou, N.; Chen, Y. B.; Li, X. W.; Xu, D.; Wang, Y.; Dong, X. R.; Cui, Y. L.; Wang, Q. Pulmonary administration of tetrandrine loaded Zinc-Alginate nanogels attenuates pulmonary fibrosis in rats. *Int. J. Pharm.* **2024**, *649*, No. 123625.
(20) Ma, L.; Liu, D.; Du, C.; Lin, L.; Zhu, J.; Huang, X.; Liao, Y.; Wu, Z. Novel NIR modeling design and assignment in process quality control of Honeysuckle flower by QbD. *Spectrochim Acta A Mol. Biomol Spectrosc* **2020**, *242*, No. 118740.
(21) An, X.; Kang, Y.; Qin, L.; Tian, Y.; Li, G. Purification of Chinese herbal extract with chitosan hydrochloride: Flocculation of single impurity and flocculation mechanism. *Korean J. Chem. Eng.* **2017**, *34* (6), 1756−1762.
(22) Lijun, C.; Boping, R.; Guorong, W.; Siyi, T.; Guishui, L. I. Flocculation Effect and Mechanism of Using Chitosan to Deal with Chinese Traditional Medicine Pudilan Water Extract. *J. Tianjin Univ. Sci. Technol.* **2016**, *31* (1), 46−50.
(23) Jin, D.; Li, L.; Dong, W.; Zhu, X.; Xia, X.; Wang, R.; Ye, J.; Li, R.; Liu, Z.; Xu, X.; Gao, L.; Liu, Y.; Wang, H. Research on Transfer Rate of Heavy Metals and Harmful Elements in Traditional Chinese Medicine Extraction and Refining Processes and Product Health Risk Assessment. *Biol. Trace Elem Res.* **2022**, *200* (4), 1956−1964.
(24) Yin, X.; Ke, T.; Zhu, H.; Xu, P.; Wang, H. Efficient Removal of Heavy Metals from Aqueous Solution Using Licorice Residue-Based Hydrogel Adsorbent. *Gels* **2023**, *9* (7), 559.
(25) Xiao, Q.; Han, J.; Jiang, C.; Luo, M.; Zhang, Q.; He, Z.; Hu, J.; Wang, G. Novel Fusion Protein Consisting of Metallothionein, Cellulose Binding Module, and Superfolder GFP for Lead Removal from the Water Decoction of Traditional Chinese Medicine. *ACS Omega* **2020**, *5* (6), 2893−2898.
(26) Fu, Q.; Zhang, T.; Sun, X.; Zhang, S.; Waterhouse, G. I. N.; Sun, C.; Li, H.; Ai, S. Pyridine-based covalent organic framework for efficient and selective removal of Hg(II) from water: Adsorption behavior and adsorption mechanism investigations. *Chem. Eng. J.* **2023**, *454*, No. 140154.
(27) Mofradi, M.; Karimi, H.; Dashtian, K.; Ghaedi, M. Corn derivative mesoporous carbon microspheres supported hydrophilic polydopamine for development of new membrane: Water treatment containing bovine serum albumin. *Chemosphere* **2020**, *259*, No. 127440.
(28) Albishri, H. M.; Yakout, A. A. Efficient removal of Hg(II) from dental effluents by thio-functionalized biochar derived from cape gooseberry (Physalis peruviana L.) leaves. *Materials Chemistry And Physics* **2023**, *295*, No. 127125.
(29) Li, Y.; Xia, M.; An, F.; Ma, N.; Jiang, X.; Zhu, S.; Wang, D.; Ma, J. Superior removal of Hg (II) ions from wastewater using hierarchically porous, functionalized carbon. *J. Hazard. Mater.* **2019**, *371*, 33−41.
(30) Bohli, T.; Ouederni, A.; Fiol, N.; Villaescusa, I. Evaluation of an activated carbon from olive stones used as an adsorbent for heavy metal removal from aqueous phases. *Comptes rendus - Chimie* **2015**, *18* (1), 88−99.
(31) Sulaymon, A. H.; Mohammed, T. J.; Al-Najar, J. Equilibrium and kinetics studies of adsorption of heavy metals onto activated carbon. *Can. J. Chem. Eng. Technol.* **2009**, *162* (3), 616−645.
(32) Mohseni, M.; Akbari, S.; Pajootan, E.; Mazaheri, F. Amine-terminated dendritic polymers as a multifunctional chelating agent for heavy metal ion removals. *Environ. Sci. Pollut Res. Int.* **2019**, *26* (13), 12689−12697.
(33) Sun, B.; Tian, H. Y.; Zhang, C. X.; An, G. Preparation of biomimetic-bone materials and their application to the removal of heavy metals. *Aiche Journal* **2013**, *59* (1), 229−240.
(34) Lu, W.; Ma, Y.; Lu, H.; Yuan, X.; Zhang, J.; Yu, M. Efficacious Removal of Trace Mercury from Honeysuckle Water Decoction Using Multifunctional Mesoporous Carbon. *ACS Omega* **2022**, *7* (50), 46787−46797.
(35) Anbia, M.; Dehghan, R. Functionalized CMK-3 mesoporous carbon with 2-amino-5-mercapto-1,3,4-thiadiazole for Hg(II) removal from aqueous media. *Journal of Environmental Sciences* **2014**, *26* (7), 1541−1548.

https://doi.org/10.1021/acsomega.4c03269
ACS Omega 2024, 9, 44931−44941

(36) Mariana, M.; Abdul, K. H. P. S.; Mistar, E. M.; Yahya, E.; Alfatah, T.; Danish, M.; Amayreh, M. Recent advances in activated carbon modification techniques for enhanced heavy metal adsorption. *J. Water Process Eng.* **2021**, *43*, No. 102221.
(37) Marciniak, M.; Goscianska, J.; Frankowski, M.; Pietrzak, R. Optimal synthesis of oxidized mesoporous carbons for the adsorption of heavy metal ions. *J. Mol. Liq.* **2019**, *276* (3), 630−637.
(38) Yin, F.; Lu, K. L.; Wei, X. Y.; Fan, Z. C.; Li, J. H.; Kong, Q. Q.; Zong, Z. M.; Bai, H. C. Fabrication of N/O self-doped hierarchical porous carbons derived from modified coal tar pitch for high-performance supercapacitors. *FUEL* **2022**, *310*, No. 122418.
(39) Wang, B.; Xu, X.; Tang, H.; Mao, Y.; Chen, H.; Ji, F. Highly efficient adsorption of three antibiotics from aqueous solutions using glucose-based mesoporous carbon. *Appl. Surf. Sci.* **2020**, *528*, No. 147048.
(40) Tzvetkov, G.; Tsyntsarski, B.; Balashev, K.; Spassov, T. Microstructural investigations of carbon foams derived from modified coal-tar pitch. *Micron* **2016**, *89*, 34−42.
(41) Saha, D.; Barakat, S.; Bramer, S. E. V.; Nelson, K. A.; Chen, J. Non-Competitive and Competitive Adsorption of Heavy Metals in Sulfur-functionalized Ordered Mesoporous Carbon. *ACS Appl. Mater. Interfaces* **2016**, *8* (49), 34132−34142.
(42) Kong, Q.; Wei, J.; Hu, Y.; Wei, C. Fabrication of terminal amino hyperbranched polymer modified graphene oxide and its prominent adsorption performance towards Cr(VI). *J. Hazard. Mater.* **2019**, *363*, 161−169.
(43) Barczak, M.; Michalak-Zwierz, K.; Gdula, K.; Tyszczuk-Rotko, K.; Dobrowolski, R.; Dąbrowski, A. Ordered mesoporous carbons as effective sorbents for removal of heavy metal ions. *Microporous Mesoporous Mater.* **2015**, *211*, 162−173.
(44) Ma, Z.; Liu, F.; Liu, N.; Liu, W.; Tong, M. Facile synthesis of sulfhydryl modified covalent organic frameworks for high efficient Hg(II) removal from water. *J. Hazard Mater.* **2021**, *405*, No. 124190.
(45) Hiremath, N.; Bhat, S.; Boy, R.; Evora, M. C.; Naskar, A. K.; Mays, J.; Bhat, G. Carbon nanofibers based carbon-carbon composite fibers. *Discovery Nano* **2023**, *18* (1), 159.
(46) Elmaghraby, N. A.; Hassaan, M. A.; Zien, M. A.; Abedelrhim, E. M.; Ragab, S.; Yılmaz, M.; El Nemr, A. Fabrication of carbon black nanoparticles from green algae and sugarcane bagasse. *Sci. Rep.* **2024**, *14* (1), 5542.
(47) Ghafuri, H.; Hanifehnejad, P.; Rashidizadeh, A.; Tajik, Z.; Dogari, H. Synthesis and characterization of nanocatalyst Cu(2+)/mesoporous carbon for amidation reactions of alcohols. *Sci. Rep.* **2023**, *13* (1), 10133.
(48) Liu, Q.; Wu, H.; Chen, J.; Guo, B.; Zhao, X.; Lin, H.; Li, W.; Zhao, X.; Lv, S.; Huang, C. Adsorption mechanism of trace heavy metals on microplastics and simulating their effect on microalgae in river. *Environ. Res.* **2022**, *214* (Pt 1), No. 113777.

https://doi.org/10.1021/acsomega.4c03269
ACS Omega 2024, 9, 44931−44941